Desalination and Water Treatment
www.deswater.com
doi: 10.1080/19443994.2015.1090924

57 (2016) 18446–18462
August

Taylor & Francis
Taylor & Francis Group

Preparation, characterization, and adsorption properties of magnetic multi-walled carbon nanotubes for simultaneous removal of lead(II) and zinc(II) from aqueous solutions

Lili Jiang[a,b,1,*], Haitao Yu[c,1], Xiaomeng Zhou[d], Xingang Hou[b], Zongshu Zou[a], Shujun Li[d], Chuantong Li[d], Xiayan Yao[d]

[a]*College of Material and Metallurgy, Northeastern University, No. 3-11, Wenhua Road, Heping District, Shenyang, Liaoning Province, P.R. China, Tel. +86 024 82681545; Fax: +86 024 83681545; emails: jianglili2002@163.com (L. Jang), zouzs@mail.neu.edu.cn (Z. Zou)*
[b]*Laboratory of Advanced Processing and Recycling of Non-ferrous Metal, Lanzhou University of Technology, No. 287, Langongping Road, Lanzhou, Gansu Province 730050, P.R. China, Tel. +86 0931 2976378; Fax: +86 0931 2976702; email: houxg1958@163.com (X. Hou)*
[c]*Department of Medical Laboratory, The First Hospital of Lanzhou University, No. 1, Donggang Road, Chengguan District, Lanzhou, Gansu Province 730000, P.R. China, Tel. +86 0931 8626421; Fax: +86 0931 8619797; email: yuhaitao7707@163.com*
[d]*School of Material Science and Technology, Lanzhou University of Technology, Langongping Road, Lanzhou, Gansu province 730050, P.R. China, Tel. +86 0931 2976378; Fax: +86 0931 2976702; email: 1018800345@qq.com (X. Zhou), L272395355@163.com (C. Li), 18215142756@163.com (X. Yao)*

Received 14 April 2015; Accepted 28 August 2015

ABSTRACT

Novel-modified magnetic multi-walled carbon nanotubes (MMWCNTs) were synthesized via evaporating acid purification and co-precipitation method. MMWCNTs were used for simultaneously removing lead and zinc ions from aqueous solutions. Transmission electron microscope, field emission scanning electron microscopy, X-ray diffraction (XRD), Fourier transform infrared spectroscopy, X-ray photoelectron spectroscopy (XPS), and magnetization curve showed the morphology, composition, surface functional groups, and magnetic properties of MMWCNTs. Then, the adsorption effects were investigated by times, pH, and adsorbent dosages. The results showed that Fe_3O_4 of approximate 10 nm successfully grafted on the surface of MWCNTs. The results of XRD, energy-dispersive X-ray spectroscopy, and XPS further confirmed that the iron oxides were Fe_3O_4. Adsorption data were analyzed with Lagergren pseudo-first-order, pseudo-second-order kinetic, intraparticle diffusion, and liquid film diffusion models. Langmuir isotherm model showed the maximum adsorption capacities as 67.25 and 3.759 mg/g for lead and zinc ions, respectively. These results indicated that MMWCNTs may be a promising candidate for removing heavy metal ions from aqueous solutions.

*Corresponding author.

[1]Lili Jiang and Haitao Yu contributed to the manuscript equally and both should be considered as 1st co-author.

Keywords: Magnetic multi-walled carbon nanotubes; Adsorption; Metal ions

1. Introduction

Heavy metal ions in water sources attract global attention because of their adverse effects on the environment as well as human health. In order to protect aquatic organisms and human from contamination, there is a need to remove heavy metal ions from aqueous solution [1]. Among the heavy metal ions that are prevalent in aquatic environments, lead and zinc ions have been most frequently researched in terms of water treatment, due to their wide-ranging presence. Lead is ubiquitous in the environment and a very toxic element. Human exposure can result in a wide range of biological effects, depending on the concentration and duration of exposure. High concentration of exposure to lead may result in poisoning and impair of the kidney, gastrointestinal tract, joints, and reproductive system [2]. General symptoms of zinc toxicity are stunted growth and edema of lungs for human beings. Hence, the removal of lead and zinc ions from water sources to an acceptable concentration is a current research challenge in water treatment and they are suitable as good pollutant models.

Many methods, such as adsorption, chemical complexation, membrane filtration, ion exchange, precipitation, and flocculation, have been widely adopted to eliminate or reduce heavy metal ions in aquatic environments [3]. Among these techniques, adsorption is the most attractive due to its simplicity, high efficiency, and its ability to remove multiple heavy metals simultaneously. Currently, carbon nanotubes (CNTs) as adsorbent have received special attention. CNTs were first created by Iijima in 1991 [4], and it mainly included single-walled CNTs (SWCNTs) and multi-walled CNTs (MWCNTs). Since MWCNTs are fibrous mesoporous structures with large specific surface area and inexpensive price, they have been in numerous applications as adsorbents [5], catalysts [6], sensors [7], electrical devices [8], supercapacitor [9], and in biotechnology [10]. In most cases, MWCNTs are hydrophobic and have poor dispersibility in the water solution due to their stable structure. These defects restrict the application of MWCNTs as adsorbent [11].

The modified MWCNTs are considered to be promising candidates to improve heavy metal adsorption. Many studies have focused on modified MWCNTs for heavy metal adsorption, such as cadmium [12], lead [13], gold [14], chromium [15], antimony [16], copper [17], and zinc [18], from aqueous solutions. In most studies, only single-adsorbate adsorption on modified MWCNTs is observed, which may not be useful for predicting contaminant sorption in wastewater because multiple contaminants, such as lead and zinc, and competitive sorption are generally present. However, information about competitive sorption between lead and zinc ions and modified MWCNTs effecting on their competitive sorption is scarce. Furthermore, separating modified MWCNTs from aqueous solution is difficult due to their improved dispersibility and strong affinity toward each other [19].

Magnetic multi-walled carbon nanotubes (MMWCNTs), combining magnetic property of iron oxide with the adsorption property of MWCNTs, have attracted tremendous interest in the world [20]. Therefore, the preparation of MMWCNTs has been given much attention. Though many synthesis methods of MMWCNTs have been reported [21–25], there are still some drawbacks, such as (1) the use of complex instrumentation, the consumption of a large amount of acids, and surfactants as well as long synthesis time; (2) the structure of MWCNTs can be destroyed by strong acids, leading to the weakened performance and the emission of toxic gases, such as carbon monoxide, in the case of the thermal decomposition method; and (3) a non-uniform distribution of particles on the MWCNTs surface. So, a facile and effective method to synthesize MMWCNTs is highly desirable. In most cases, MWCNT is modified by acid wash such as dissolving in HNO_3, H_2SO_4, or a mixture of these acids [26,27]. Acid wash method has limitations on adding containing oxygen groups to the MWCNT walls, and can damage the MWCNT structure, affecting the consistency of the sorption results.

The main objectives of this study are to solve above problems and investigate the adsorption capacity of the composite. The composite was synthesized via evaporating acid purification and co-precipitation method. Adsorption capacity of the composite was investigated under several parameters such as time, pH, and adsorbent dosages. The kinetics fitted the adsorption data by pseudo-first-order, pseudo-second-order kinetic, intraparticle diffusion, and liquid film diffusion models. Adsorption isotherm experiments were conducted to determine maximal adsorption capacity of the composite for lead and zinc ions. Adsorption mechanisms provided theoretical foundations for removing of heavy metal from the water solutions.

2. Materials and method

2.1. Materials and reagents

MWCNTs (outer diameter: 10–30 nm; length: 5–15 μm; purity: ≥95%) were purchased from Shenzhen Nanotech Port Co. Ltd, (China). Lead nitrate, zinc nitrate, ammonium ferrous sulfate ($(NH_4)_2Fe(SO_4)_2{\cdot}6H_2O$), and ammonium ferric sulfate ($NH_4Fe(SO_4)_2{\cdot}12H_2O$) were purchased from Sinopharm Chemical Reagent Co. Ltd, (China). All chemicals were analytical grade and used as received without further purification.

2.2. Characterization methods

The morphologies of the samples were observed by a transmission electron microscope (TEM, JSM-6701F, Japan Electron Optics Laboratory). A field emission scanning electron microscope (FESEM, Quanta FEG-450) was used to detect the morphology of the synthesized products. Energy-dispersive X-ray spectroscopy (EDS) attached to FESEM was used for elemental analysis. X-ray diffraction (XRD) patterns were obtained using an X-ray diffractometer (D8-ADVANCE) with CuKα as the X-ray radiation source to identify the phase structure. The Fourier transform infrared (FTIR) spectrum was performed by a Fourier transform infrared spectrometer (Nexus 870, Nicolet). Surface element compositions were assessed by an X-ray photoelectron spectroscopy (XPS, ESCALAB 210, British VG Scientific) by monochromatic AlKa radiation. The magnetic property was investigated using a vibrating sample magnetometer (VSM, Lakeshore 7304). Metal ion concentrations were analyzed by an atomic absorption spectrophotometer (HITACHI Z-5000). A temperature-controlled shaker was used for shaking the aqueous solution containing metal ions and a temperature-controlled water bath (HHS2) was used for maintaining the temperature of aqueous solution.

2.3. Preparation of oxidized MWCNTs

One gram of MWCNTs was placed into a sand core funnel, and then the funnel was inserted into a container containing 10 mL of concentrated nitric acid. The container was placed in a reactor and sealed. The reactor was slowly heated to 200°C for 4 h. The sand core funnel was taken out after cooling to room temperature, washed by deionized water for several times, and then dried at 80°C in a vacuum oven for 5 h. Finally, the black samples were obtained, which were oxidized MWCNTs (o-MWCNTs).

2.4. Synthesis of Fe_3O_4/o-MWCNTs

Fe_3O_4 nanoparticles were prepared by co-precipitation method. First, 1.7 g of $(NH_4)_2Fe(SO_4)_2{\cdot}6H_2O$ and 2.51 g of $NH_4Fe(SO_4)_2{\cdot}12H_2O$ were added in 200 mL of deionized water and dissolved by strong stir. Then 1.0 g of o-MWCNTs was dispersed in the mixed solution followed by ultrasonic treatment for 30 min. Subsequently, 8 mol/L NH_4OH was added dropwise to precipitate iron oxides and stirred for 30 min. The final mixture was adjusted to pH 11 and then allowed to react for 2 h. All of the above experiments were maintained at 50°C under a high-purity nitrogen atmosphere [28]. The mixture was cooled to room temperature after the reaction. After the resulting solid was separated from the mixture by a magnet, it was washed by deionized water for several times and dried in a vacuum oven at 80°C for 12 h. The obtained sample was Fe_3O_4/o-MWCNTs.

2.5. Batch adsorption experiments

Stock solutions of 1,000 mg/L lead and zinc ions were prepared by, respectively, dissolving 1.60 g of $Pb(NO_3)_2$ and 2.90 g of $Zn(NO_3)_2$ in 1,000 mL of Milli-Q water. These stock solutions were acidified with approximately 2 mL of concentrated HNO_3 to prevent hydrolysis of lead and zinc ions and then further diluted with Milli-Q water to the required concentrations before being used. In order to investigate the effects of pH on the adsorption capacities, for each solution, 50 mg of Fe_3O_4/o-MWCNTs were suspended in 50 mL of solution with 30 mg/L zinc and 200 mg/L lead. The conical flasks were shaken for 6 h with pH values (from 1.0 to 5.0) at 25°C. Subsequently, 10.0 mL of solution was pipetted out from each conical flask and filtered through 0.45-μm polytef membranes. The concentration of lead and zinc ions in the supernatant was immediately analyzed by atomic absorption spectrophotometer. All adsorption experiments were performed in triplicate, and the averaged values were reported in this study. The adsorption capacity was calculated using the following equation:

$$q_t = (C_0 - C_t)\frac{V}{m} \tag{1}$$

where q_t is the amount of metal ions adsorbed by per unit mass of adsorbent (mg/g); C_0 and C_t are the metal ion concentrations in the initial solution and after time t (mg/L), respectively; m represents the weight of the adsorbent (g), and V is the volume of solution (L).

The removal rate (%) was calculated using the following equation:

$$\text{removal rate}\,(\%) = \frac{(C_0 - C_t)}{C_0} \times 100\% \quad (2)$$

The effects of contact time on the adsorption capacity were studied in solutions containing 30 mg/L zinc and 200 mg/L lead with pH 5.0 at 25˚C. Fifty milligrams of adsorbents were dispersed into 50 mL of solutions in a 100-mL conical flask. Then at predetermined time interval (from 15 min to 12 h), 10 mL of solution was withdrawn by a syringe and filtered by 0.45-μm polytef membrane filters. The residual concentrations of lead and zinc ions in the filtrate were analyzed.

All isotherms were obtained using a batch equilibration technique at 25 ± 1˚C. The sorption isotherm experiments were performed in flasks containing zinc ions of 30 mg/L and lead ions of 200 mg/L. The amount of Fe_3O_4/o-MWCNTs varied from 10 to 70 mg at pH 5.0 for 6 h.

3. Results and discussion

3.1. Morphology and structure analysis

To explore the morphology and dimension of Fe_3O_4/o-MWCNTs, TEM was used at various magnifications. Fig. 1 shows the representative TEM images of MWCNTs, oxidized MWCNTs, and Fe_3O_4/o-MWCNTs. Fig. 1(a) shows that MWCNTs were cylindrical shapes with smooth surfaces and outer diameter approximately was 30 nm, which accorded with the values reported by the manufacturer. Little metal impurity was shown outside of MWCNTs. On the contrary, the oxidized MWCNTs had no impurities, the surface was rough with lots of grooves and the ends were opened in Fig. 1(b) and (c) shows that some Fe_3O_4 nanoparticles with an average particle size of 10–20 nm were deposited on the surface of oxidized MWCNTs. Their size distribution was evaluated by statistical diameter measurement using Nano measurer software invented in the Fudan University according to selected TEM images. The latter indicated size of Fe_3O_4 mainly was between 10 and 20 nm. There was little vacant area on the surface of oxidized MWCNTs, indicating the high efficiency of synthesis method. Although the composites had been sonicated in ethanol and distilled water for 15 min before the TEM measurements, the large amount of iron oxide nanoparticles on the oxidized MWCNTs surface indicated strong interactions between MWCNTs and iron oxides. Fe_3O_4/o-MWCNTs were strong enough to resist mechanical energy, such as manual shaking or sonication. Due to the production of oxygenous groups in the evaporating acid process, MWCNTs' surface was negatively charged. The ferric ions with positive charge adsorbed onto oxidized MWCNTs through electrostatic attractions [29]. Fig. 1(d) shows a TEM image that was taken from the circular region of Fig. 1(c). The Fe_3O_4 was approximately 10 nm. The lattice fringes with an inter-plane distance of 0.49 nm came from the (1 1 1) plane of Fe_3O_4 and they belonged to the face-centered cubic structure with lattice parameter of 8.44.

SEM images of MWCNTs, oxidized MWCNTs, and Fe_3O_4/o-MWCNTs are shown in Fig. 2. The morphology of MWCNTs and oxidized MWCNTs had not significant difference. Both types of MWCNTs were rope-like, curved, and highly tangled (Fig. 2(a) and (b)). It can be clearly seen that oxidized MWCNTs with uniform size and tubular structure had been fabricated, implying minimal damage to the tube structure under oxidized treatment. The length of these nanotubes was approximately 5–15 μm, and the average outer diameter was 10–30 nm. Fig. 2(c) shows that the surface of Fe_3O_4/o-MWCNTs was rough due to some nanoparticles attaching to o-MWCNTs surface. To further confirm the nanoparticles' composition on Fe_3O_4/o-MWCNTs surface in Fig. 2(c), EDS was employed. Fig. 2(d) confirms the presence of C, O, and Fe elements on the Fe_3O_4/o-MWCNTs surface. The C signal originated from oxidized MWCNTs, and the Fe signal came from the Fe_3O_4 nanoparticles. The results revealed the existence of Fe_3O_4, which was consistent with the results of XRD and XPS. Because MWCNTs are non-conducting, we sprayed gold on the surface of Fe_3O_4/MWCNTs. Moreover, the molar ratio of Fe and O was calculated according to the EDS and the result was closed to Fe_3O_4. This further indicated that nanoparticles on the surface of o-MWCNTs were Fe_3O_4.

To further understand the obtained adsorbent, XRD was carried out and the patterns are presented in Fig. 3. Fig. 3(a) shows two strong peaks at 26.4˚ and 42.8˚, which were assigned to the (0 0 2) and (1 0 0) planes of MWCNTs. The diffraction peak at 42.8˚of oxidized MWCNTs was weaker in Fig. 3(b) and indicated that structure of MWCNTs was damaged during the oxidized process. The XRD pattern of Fe_3O_4/o-MWCNTs showed that (0 0 2), (1 0 0) planes became weaker and illustrated that crystallinity of Fe_3O_4/o-MWCNTs had reduced significantly than oxidized MWCNTs. Fig. 3(c) shows that the XRD pattern of Fe_3O_4/o-MWCNTs matched well with the standard cubic phase of Fe_3O_4, including that the seven diffraction peaks (2θ = 30.19˚, 35.60˚, 43.21˚, 53.55˚, 57.09˚,

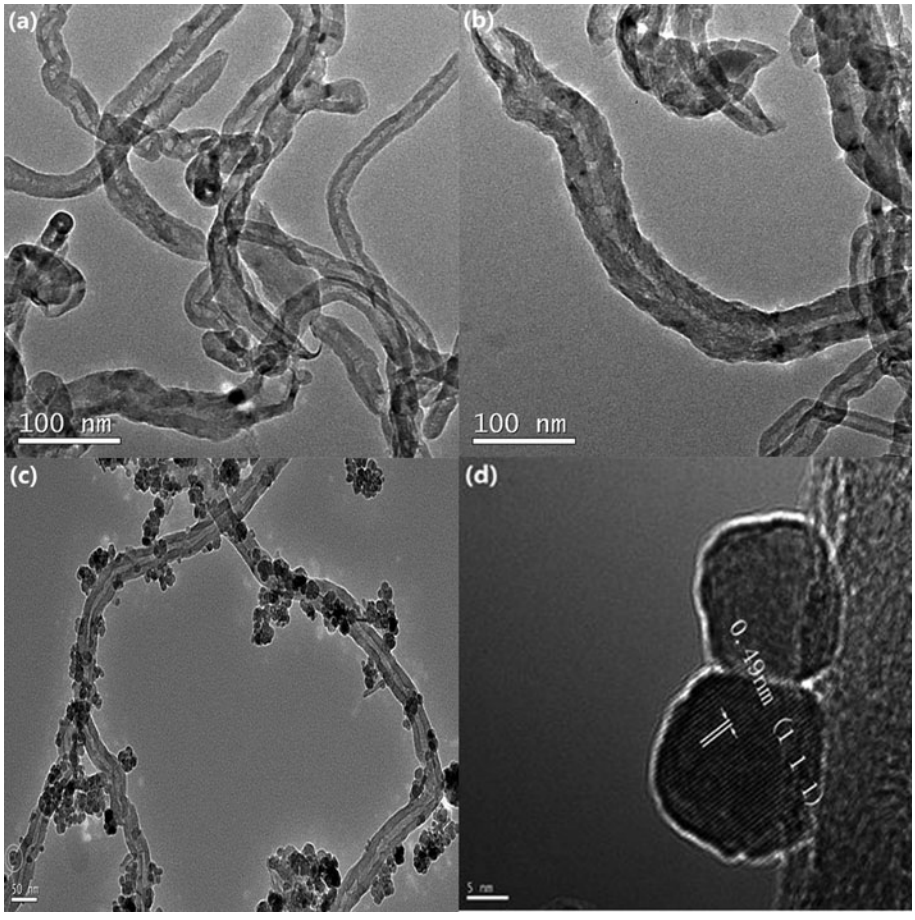

Fig. 1. Representative TEM images of (a) MWCNTs, (b) oxidized MWCNTs, (c) Fe_3O_4/o-MWCNTs, and (d) a high magnification image of Fe_3O_4.

62.70°, and 74.23°) correspond to the (2 2 0), (3 1 1), (4 0 0), (4 2 2), (5 1 1), (4 4 0), and (5 3 3) planes (JCPDS No. 19-0629) of the spinel cubic structure of magnetite, respectively. The relatively broad diffraction peaks indicated that Fe_3O_4/o-MWCNTs had a quite small crystal size [30]. We applied the Scherer equation according to the highest intensity (3 1 1) and estimated the crystallite size to be approximately 10 nm, which was consistent with result of TEM (Fig. 1(d)). In addition, it was noticed that the XRD pattern of Fe_3O_4 was quite similar with γ-Fe_2O_3 because both of phases displayed the same spinel structure [31]. Further information of the Fe_3O_4 nature of the iron oxide can be evaluated by following tests. The nitrogen environment prevented Fe_3O_4 to translate γ-Fe_2O_3. The black color of the product further testified that it solely contained the magnetite phase but not maghemite which would be brown in color. Then, there was not weak peaks in the low-angle region which corresponded to (1 1 0), (2 1 0), and (2 1 1) planes of γ-Fe_2O_3. This illustrated the existence of pure Fe_3O_4. According to the XRD and SEM results, the nanoparticles on the MWCNTs' surface were assigned to Fe_3O_4.

3.2. FTIR spectra

FTIR spectra were a standard method for the characterization of functionalized MWCNTs [32]. Fig. 4 shows the FTIR spectra of MWCNTs, oxidized MWCNTs, and Fe_3O_4/o-MWCNTs. MWCNTs showed a weak peak at 1,559 cm^{-1} associated with C=C stretching vibration (Fig. 4(a)). Fig. 4(b) illustrates that evaporating acid treatment introduced many functional groups on the surface of MWCNTs. Evidence of the C–O stretching vibration peak at 1,074 cm^{-1} was shown in the FTIR spectra (Fig. 4(b)) [27]. The oxidized treatment produced hydroxy groups on the external surface of MWCNTs, which was confirmed by the peaks of −OH stretching vibrations at 3,200–3,435 cm^{-1} [13]. Fig. 4(c) shows a broad peak

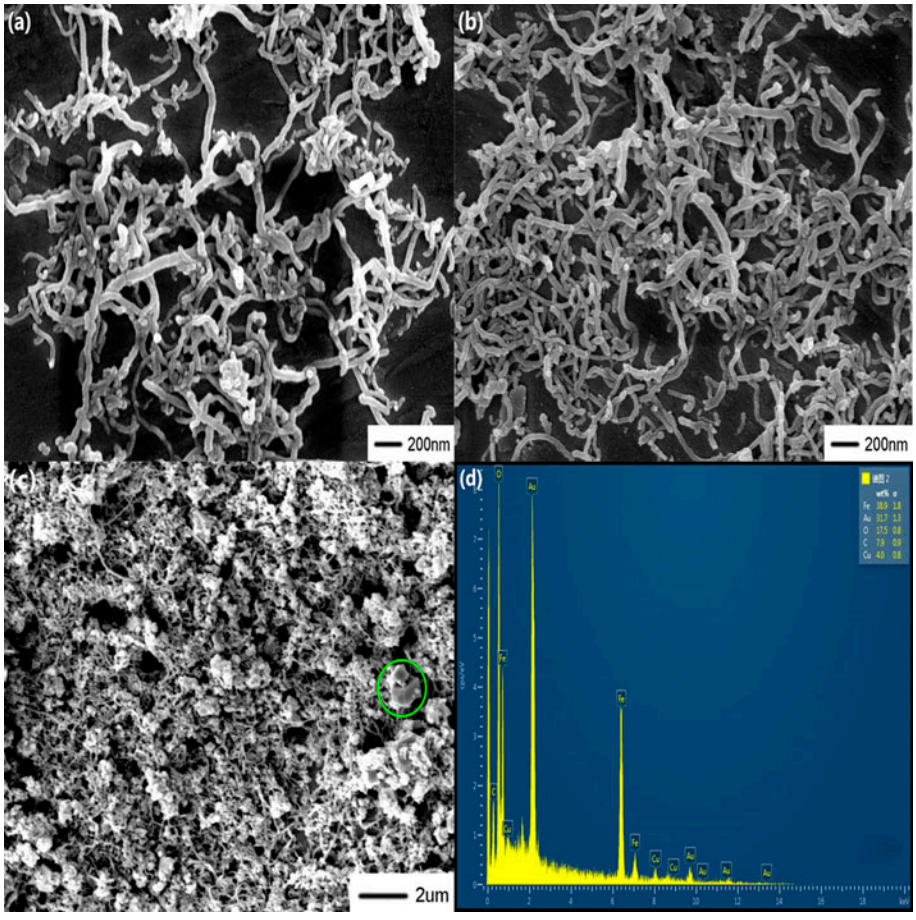

Fig. 2. SEM images of (a) MWCNTs, (b) oxidized MWCNTs, (c) Fe_3O_4/o-MWCNTs, and (d) EDS of in the circle of Fe_3O_4/o-MWCNTs.

attributed to Fe–O stretching at 599 cm^{-1}, which indicated Fe_3O_4 successfully loaded on oxidized MWCNTs [21]. The functional groups provided a large number of chemical adsorption sites and therefore increased the adsorption capacity of Fe_3O_4/o-MWCNTs. Meanwhile, the hydrophilic properties of these functional groups improved the dispersivity of Fe_3O_4/o-MWCNTs in aqueous solution.

3.3. XPS spectra

XPS was used to investigate surface element compositions and chemical states of adsorbent [17]. Fig. 5(a) shows the wide scan spectrum of the sample. The strong C 1s peak at 284.6 eV corresponded to CNTs, and the photoelectron lines at binding energies of approximately 531.02 and 64.33 eV were attributed to O 1s and Fe 3p, respectively. To determine the chemical components of Fe_3O_4/o-MWCNTs, Fig. 5(b) shows C 1s spectrum was curve fitted into two individual peaks C–C (284.7 eV) and C–OH (285.5–285.8 eV) according to possible chemical bonds and electronegativity. The presence of these oxygenous functional groups confirmed that the surfaces of MWCNTs had been successfully modified by oxidation, which provided anchors for the immobilization of Fe_3O_4. Fig. 5(c) shows the O 1s spectrum was fitted with two symmetrical peaks: the peak at 532.19 eV was assigned to the oxygen in the carboxyl groups (C=O) and the peak at 529.94 eV was from oxygen in the hydroxyl (C–O). The Fe_3O_4/o-MWCNTs showed obvious oxygen peaks in the spectrum, indicating that the evaporating acid treatment introduced oxygen-containing functional groups on the surface of MWCNTs, which was in agreement with the result of FTIR. XPS spectrum of Fe 2p is shown in Fig. 5(d). The binding energies at 710.6 and 724.6 eV corresponded to Fe $2p_{3/2}$ and Fe $2p_{1/2}$ in Fe_3O_4, respectively. There were no obvious shake up satellite structures at the higher binding energy side of both

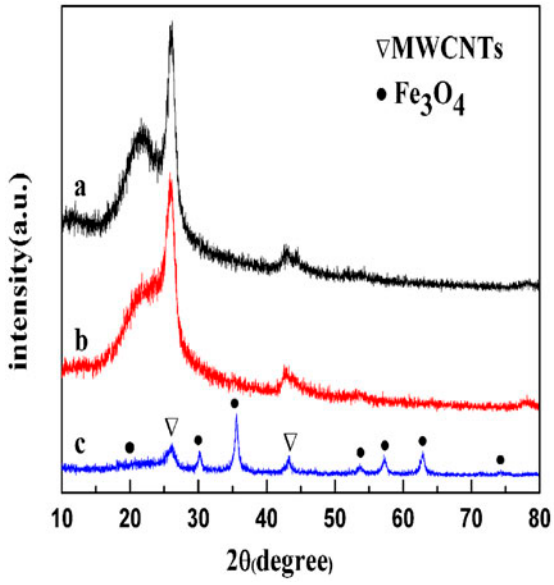

Fig. 3. XRD patterns of MWCNTs (a), oxidized MWCNTs (b), and Fe_3O_4/o-MWCNTs (c).

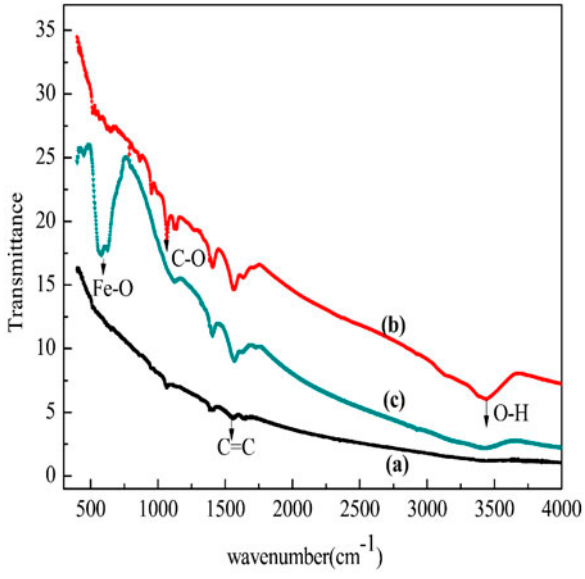

Fig. 4. FTIR spectra of MWCNTs (a), oxidized MWCNTs (b), and Fe_3O_4/o-MWCNTs (c).

main peaks (about 718.8 and 729.5 eV), which was the characteristic of Fe_3O_4 [33]. The relative area ratio of Fe $2p_{3/2}$ peak assigned to Fe^{2+} and Fe^{3+} was calculated to be 0.35:0.65, given in Table 1. Since Fe_3O_4 could also be expressed to be $FeO{\cdot}Fe_2O_3$, the Fe^{2+}:Fe^{3+} ratio should be 1:2 or 0.33:0.67. This result suggested that the Fe species were predominantly in the form of Fe_3O_4 and was consistent with the results of XRD. Furthermore, the area ratio, atomic content, mass content fraction of C, O, and Fe elements are shown in Table 1. The mass contents were C 1s:O 1s:Fe 2p = 0.82:0.11:0.07, which implied the weight fraction of Fe_3O_4 on the surface of Fe_3O_4/o-MWCNTs was 14.20%.

3.4. Separability, stability, and magnetic characterizations of Fe_3O_4/o-MWCNTs

Magnetization curve of Fe_3O_4/o-MWCNTs prepared at 298 K was characterized by a vibrating sample magnetometer, and the result is shown in Fig. 6. The saturation magnetization of Fe_3O_4/o-MWCNTs was 50.10 emu/g. There was no remanence and coercivity indicating Fe_3O_4/o-MWCNTs were superparamagnetic. Furthermore, compared with pure Fe_3O_4 nanoparticles [34], saturation magnetization of Fe_3O_4/o-MWCNTs was reduced due to the existence of MWCNT. The reason might be that Fe_3O_4 nanoparticles of superparamagnetism were attached on the surface of oxidized MWCNTs. The large saturation magnetization allowed for a fast separation of Fe_3O_4/o-MWCNTs from aqueous solution.

Stability of Fe_3O_4/o-MWCNTs in deionized water was investigated. Two milligrams of Fe_3O_4/o-MWCNTs were dispersed in 4 mL of deionized water and used for ultrasonic treatment for 10 min. Fig. 6(a) shows that Fe_3O_4/o-MWCNTs had very good stability to form a uniform black suspended solution and can be maintained for at least a few days without aggregation and precipitation which might be attributed to their improved solubility. Fig. 6(b) illustrates that nearly all of the Fe_3O_4/o-MWCNTs can be easily collected and separated from the aqueous solution by a magnet. Hence, these experimental results indicated that MWCNTs were effectively modified into Fe_3O_4/o-MWCNTs with higher stability and better separability in aqueous solution. This will benefit the separation and recycle of Fe_3O_4/o-MWCNTs from water solution.

3.5. Adsorption performance

3.5.1. Effects of pH on adsorption

The pH of solution had been consistently considered to be one of the most important variables in adsorption experiments and it controlled the surface charges of adsorbents and the species of the adsorbates. At high pH over 5, lead hydroxide became predominant and subsequently the precipitation of lead hydroxide occurred. And at pH lower than 8, the predominant zinc species was always Zn^{2+} [35,36].

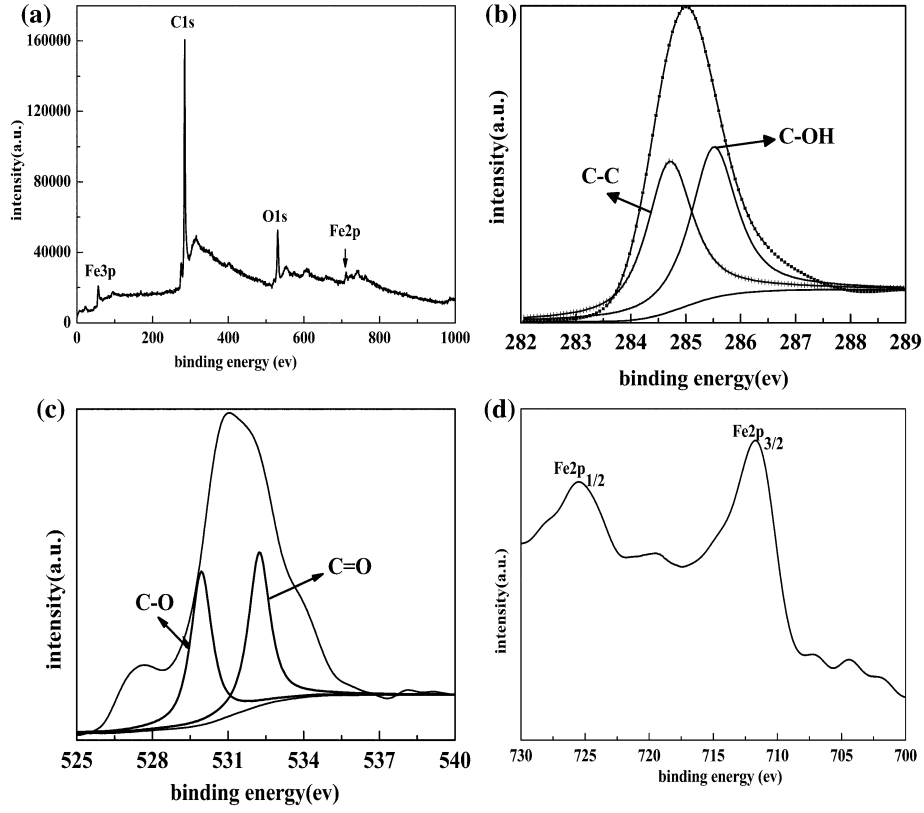

Fig. 5. XPS wide scan of Fe_3O_4/o-MWCNTs (a), C 1s spectrum (b), O 1s spectrum (c), and Fe 2p spectrum (d).

Table 1
The atomic content, mass content of Fe, C, and O elements of Fe_3O_4/o-MWCNTs

		Energy (eV)	Area (%)	Atomic content (%)	Mass content(%)
Fe 2p	Fe^{2+}	712.10	35.30	2.50	10.28
	Fe^{3+}	710.60	64.70		
C 1s	C–C	284.70	38.78	89.58	82.45
	C–OH	285.50	61.22		
O 1s	C–O	529.94	47.78	9.15	10.75
	C=O	532.19	52.21		

Thus, the adsorption experiments were conducted by varying the solution pH over the range of 1.0–5.0 to avoid the contribution from lead and zinc hydroxide precipitation. Fig. 7 shows that equilibrium adsorption capacity (q_e) of Fe_3O_4/o-MWCNTs was highly dependent on pH. The equilibrium adsorption capacity increased gradually with increasing pH. Fig. 7(a) illustrates that removal rate began to increase gradually until pH 5 with q_e of 49.57 mg/g and reached a maximum removal rate of 25%. Moreover, Fe_3O_4/o-MWCNTs had a lower removal rate for Zn^{2+} (7.93%) and equilibrium adsorption capacity was 2.38 mg/g at pH 5. To investigate the effect of lead adsorption on zinc adsorption, the experiments under lead–zinc dual system were conducted. The equilibrium adsorption capacity for zinc ions in a sole Zn^{2+} system was 15.78 mg/g at pH 5 with high removal rate (52.6%) and is shown in Fig. 7(c). Compare with those in lead–zinc dual system, the values increased. The results indicated lead adsorption in the lead–zinc dual system prevented zinc adsorption.

The results revealed that equilibrium adsorption capacity was in the order of lead ion > zinc ion. This can be explained that radius of lead ion (1.2 Å) was greater than zinc ion (0.74 Å) and the aqua complex of lead ion ($Pb(H_2O)_6^{2+}$) can directly compete with zinc

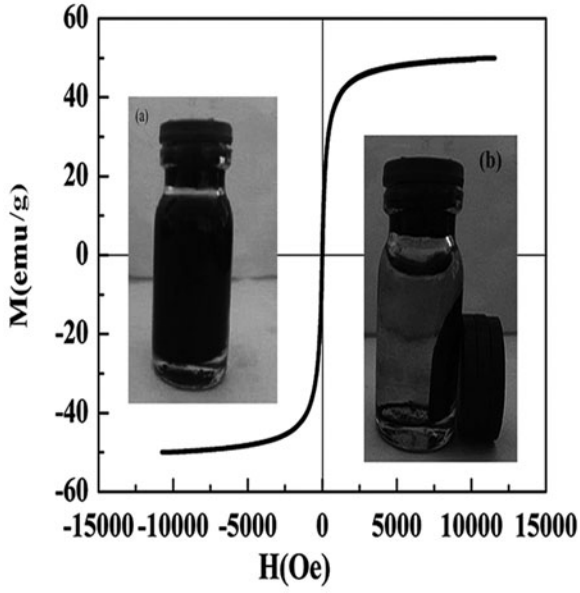

Fig. 6. Magnetization curve of Fe_3O_4/o-MWCNTs and insets of stability (a) and separation process (b) of Fe_3O_4/o-MWCNTs.

ion ($Zn(H_2O)_6^{2+}$) for sorption sites through squeezing, occupying, and shielding part adsorption sites on MWCNTs surface [37]. Pb^{2+} and $Pb(H_2O)_6^{2+}$ can occupy more adsorption sites, thus, adsorption capacity of lead ion was greater than zinc ion. The equilibrium adsorption capacity was very weak at pH lower than 2, due to the competition of H_3O^+ for available surface-binding sites. The isoelectric point was 2.85 for nitric acid-oxidized MWCNTs. Under basic conditions (pH higher than 2.85), Fe_3O_4/o-MWCNTs was negatively charged. The lone pairs of electrons on oxygen atom were available to interact with lead and zinc ions through electrostatic interactions.

3.5.2. Effects of contact time and adsorption kinetics

The effects of contact time on the adsorption capacity of Fe_3O_4/o-MWCNTs were studied by measuring the extent of adsorption at different time intervals at 25°C. Adsorption kinetics was important for understanding the rate processes involved in the removal rate of heavy metals from aqueous solutions. The adsorption kinetics data of metal ions

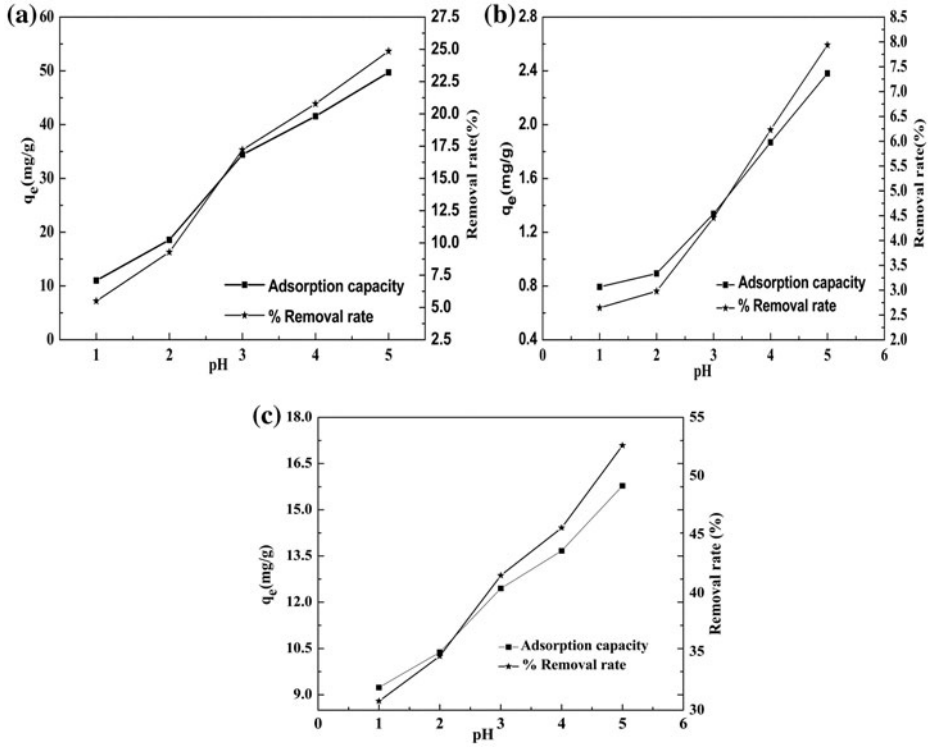

Fig. 7. Effects of pH on equilibrium adsorption capacity and removal rate of lead (a) and zinc (b) in lead–zinc dual system and zinc in a sole zinc system (c).

on Fe_3O_4/o-MWCNTs surface was fitted by different kinetic models: Lagergren pseudo-first-order model, pseudo-second-order model, the intraparticle diffusion model, and the liquid film diffusion model. The equation of pseudo-first-order kinetics was given by [38]:

$$\ln(q_e - q_t) = \ln q_e - k_1 t \quad (3)$$

where k_1 (1/min) is the pseudo-first-order adsorption rate coefficient and q_e is the amount of metal ions adsorbed per unit mass at equilibrium. The plots of $\ln(q_e - q_t)$ vs. t for lead and zinc ions are not shown. The linear form of pseudo-second-order rate equation was given as [39]:

$$\frac{t}{q_t} = \frac{1}{k_2 q_e^2} + \frac{t}{q_e} \quad (4)$$

where k_2 (g/mg/min) is the pseudo-second-order rate constant and q_t is the amounts of metal ions adsorbed per unit mass at time t.

The kinetics of lead and zinc ions adsorption on Fe_3O_4/o-MWCNTs surface was studied, and the resulting pseudo-second-order kinetics plots are shown in Fig. 8. The adsorption capacities of Fe_3O_4/o-MWCNTs for lead and zinc ions increased with increasing time, and Fe_3O_4/o-MWCNTs exhibited high adsorption capacity (Fig. 8(a) and (c)). Fig. 8(a) illustrates the adsorption capacity of Fe_3O_4/o-MWCNTs for lead ions increased rapidly for short contact times of 15 min, and then followed by a slow and steady increase until near saturation. Fig. 8(c) shows adsorption capacity of Fe_3O_4/o-MWCNTs markedly increased with increasing time and reached equilibrium at 360 min. The short adsorption equilibrium time indicated that Fe_3O_4/o-MWCNTs had high adsorption efficiency for industrial application. The kinetics curves were smooth and continuous, leading to saturation, suggesting the possibility of the formation of monolayer coverage of lead and zinc ions on Fe_3O_4/o-MWCNTs surface. The initial high adsorption capacity may be attributed to more bare surfaces of Fe_3O_4/o-MWCNTs. Lead and zinc ions occupied the active surface sites at random. With increasing of contact time, the number of available adsorption sites decreased, and adsorption rate became slower in the latter stage. Ultimately, the surface of Fe_3O_4/o-MWCNTs became saturated and reached the saturation adsorption. Since equilibrium was reached within 6 h, the contact time for adsorption studies was maintained at 6 h throughout all the experiments.

Fig. 8(b) and (d) shows the pseudo-second-order kinetics plots. Linear plots of this process indicated that lead and zinc ions adsorption accorded with pseudo-second-order rate expression. The pseudo-first- and pseudo-second-order rate equation parameters are listed in Table 2. It was clear that the experimental data fitted the pseudo-second-order equation with higher correlation coefficient ($R^2 \geq 0.998$), indicating the suitability of pseudo-second-order rate equation. In addition, the equilibrium adsorption capacities were 50.71 and 2.394 mg/g for lead and zinc ions, respectively. The data were much closer to the experimental values (q_e = 46.85, 2.35 mg/g) than pseudo-first-order model (7.87, 0.713 mg/g), respectively. The rate constant K_2 was 3.32×10^{-3} for Pb^{2+} and 1.98×10^{-3} (g/mg/min) for Zn^{2+}, indicating that the adsorption rate of lead ion was faster than zinc ion.

The intraparticle diffusion model was expressed as follow:

$$q_t = K_{id} t^{\frac{1}{2}} + C_i \quad (5)$$

where q_t is adsorption capacity at time t (mg/g); K_{id} is the intraparticle diffusion rate constant (mg/g/min$^{0.5}$); and C_i (mg/g) is a constant proportional to the thickness of the boundary layer. Parameters of intraparticle diffusion model are shown in Table 3 and correlation coefficients (R^2) were not good. Fig. 9(a) and (b) shows that the lines did not pass through the origin, although middle plot lines were lying in a straight line. It indicated that the intraparticle diffusion model was involved in the adsorption process but not the only the rate-determining step.

Liquid film diffusion was another kinetic model that assumed that the flow of the adsorbate molecules through a liquid film surrounding the solid adsorbent was the slowest step in the adsorption process and determined the kinetics of the rate processes. The liquid film diffusion model is shown as follow [40]:

$$\ln(1 - F) = -K_{fd} \times t \quad (6)$$

where F is the ratio of adsorption capacity at time t and equilibrium ($F = q_t/q_e$) and K_{fd} (1/min) is the film diffusion rate coefficient. A linear plot of $-\ln(1 - F)$ vs. t with zero intercept suggests that the kinetics of the adsorption process was controlled by diffusion through the liquid film around Fe_3O_4/o-MWCNTs.

Fig. 10 shows that the application of the liquid film diffusion model to the lead and zinc ions adsorption by Fe_3O_4/o-MWCNTs converged well, as the correlation coefficients were 0.984 and 0.912 but had non-zero intercepts (1.93 and 0.589) against the predictions of the model (Table 3).

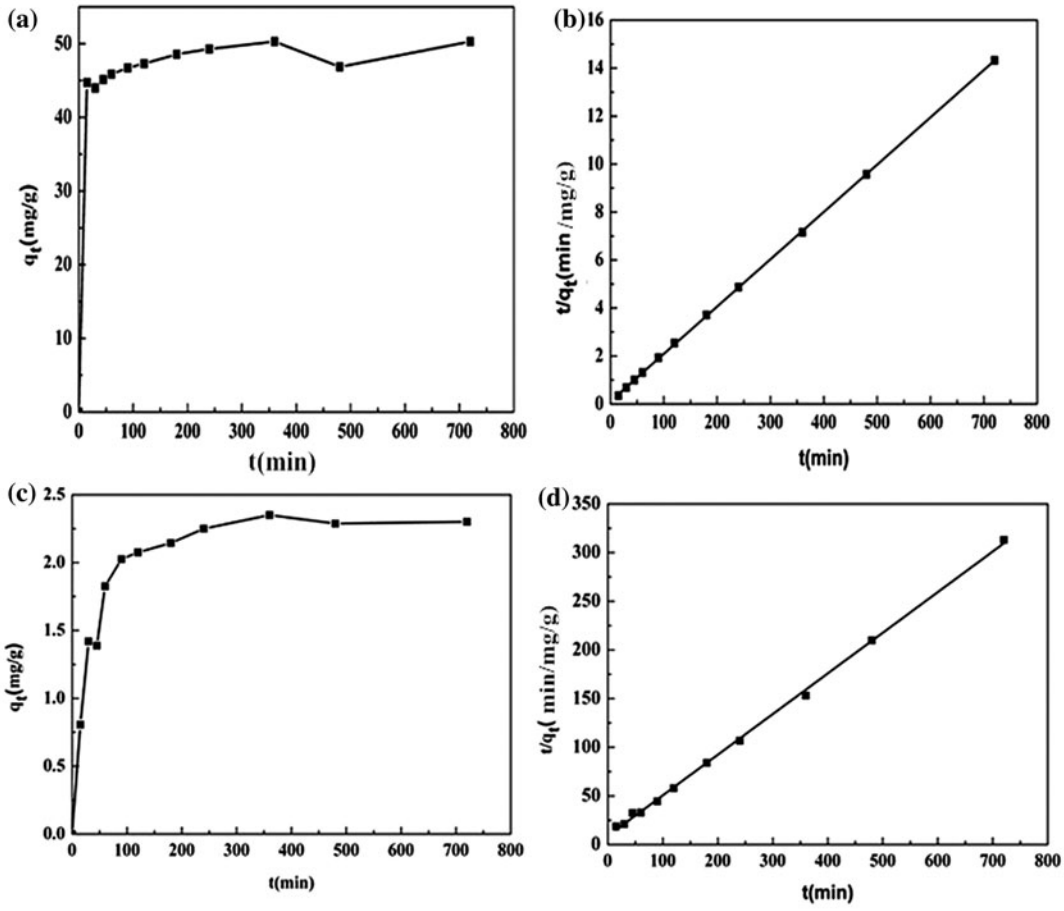

Fig. 8. Effects of contact time on lead (a) and zinc adsorption (c) and pseudo-second-order kinetics plots of lead (b) and zinc (d) adsorption.

Table 2
Pseudo-first-and pseudo-second-order rate equation parameters for lead and zinc ions adsorption on Fe_3O_4/o-MWCNTs (experimental conditions: temperature, 298 K; pH 5.0; Fe_3O_4/o-MWCNTs mass, 1 g/L; Zn^{2+} concentration of 30 mg/L and Pb^{2+} concentration of 200 mg/L)

	Model	q_e (mg/g)	k_1 or k_2 (1/min or g/mg/min)	R^2	Experimental q_e (mg/g)
Pb^{2+}	Pseudo-first-order	7.87	8.55×10^{-3}	0.995	46.85
Zn^{2+}		0.713	4.55×10^{-3}	0.749	2.35
Pb^{2+}	Pseudo-second-order	50.71	3.32×10^{-3}	0.999	46.85
Zn^{2+}		2.394	1.98×10^{-3}	0.998	2.35

3.5.3. Adsorption isotherms

The adsorption isotherm model was typically used to fit experimental data and help to explore the adsorption mechanism more deeply. The Langmuir and Freundlich isotherm models were the most conventional models among the abundant isotherm models. The Langmuir isotherm described a homogeneous monolayer adsorption, meaning that all of the adsorption sites had equal adsorbates affinity and is expressed as follows [41]:

$$\frac{1}{q_e} = \frac{1}{bq_m C_e} + \frac{1}{q_m} \tag{7}$$

where C_e is the equilibrium concentration of metal ions in solution (mg/L), q_e is the adsorbed value of

Table 3
Parameters of intraparticle diffusion and the liquid film diffusion model

	Intraparticle diffusion			Liquid film diffusion	
	K_{id} (mg/g/min$^{0.5}$)	C_i (mg/g)	R^2	K_{fd} (1/min)	R^2
Pb^{2+}	0.328	43.132	0.85186	0.008	0.984
Zn^{2+}	0.054	1.203	0.607	0.011	0.912

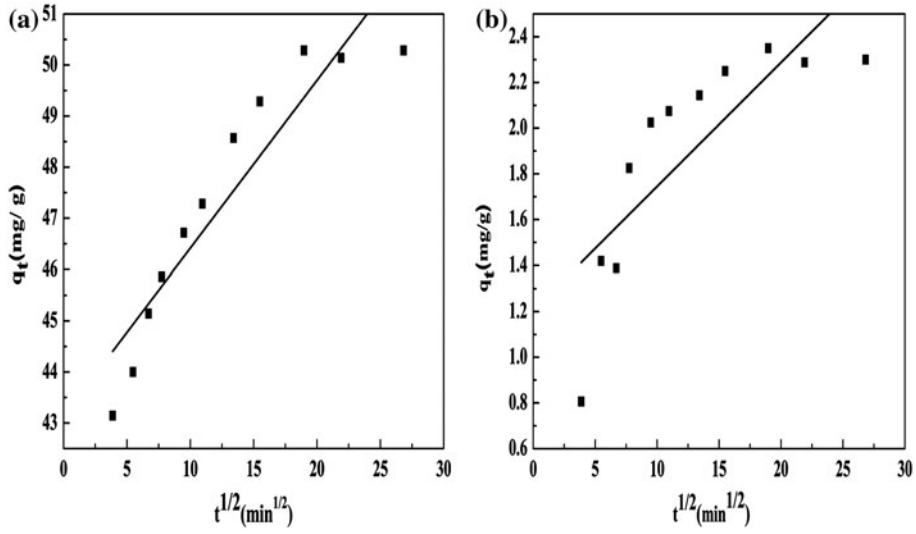

Fig. 9. Intraparticle diffusion model plots of lead (a) and zinc ions (b) adsorption on the Fe_3O_4/o-MWCNTs surface.

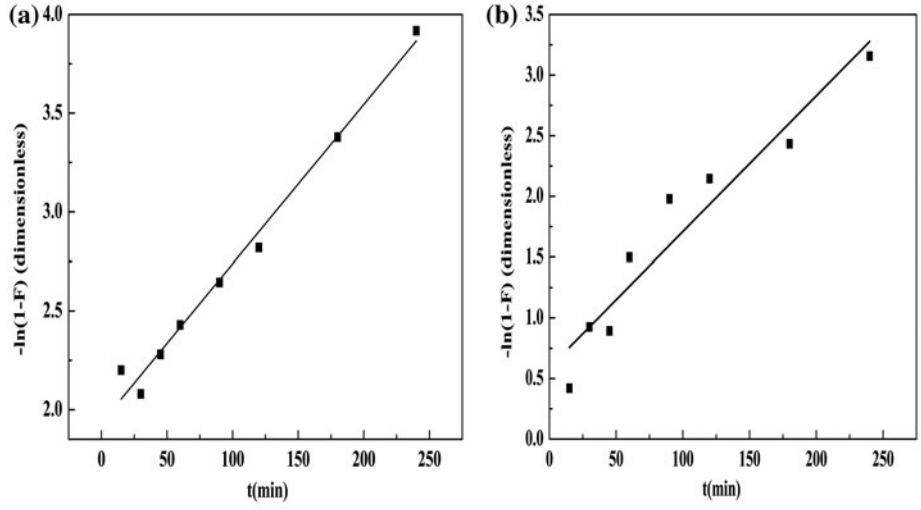

Fig. 10. Liquid film diffusion model of lead (a) and zinc (b) adsorption on the Fe_3O_4/o-MWCNTs surface.

metal ions at equilibrium concentration (mg/g), q_m and b are the maximum adsorption capacity (mg/g) and energy of adsorption (L/mg), respectively. The values of q_m and b were obtained from the intercept and the slope of the linear plot of $1/q_e$ against $1/C_e$.

The efficiency of adsorption can be expressed by the dimensionless equilibrium parameter R_L, which is defined as follows:

$$R_L = \frac{1}{1+bC_0} \tag{8}$$

where b is the Langmuir constant (L/mg) and C_0 is the initial lead and zinc concentration (mg/L). The values of R_L indicated the isotherm shape was unfavorable ($R_L \geq 1$) or favorable ($0 \leq R_L \leq 1$).

The Freundlich isotherm model assumed the multilayer adsorption was heterogeneity. It can be described as follows [42]:

$$\ln q_e = \ln K_f + \frac{1}{n}\ln C_e \tag{9}$$

where K_f [$(mg)^{1-1/n}(L)^{1/n}/g$] is the adsorption capacity as the equilibrium metal ion concentrations were equal; n represents the degree of dependence of adsorption on the equilibrium concentration.

Figs. 11 and 12 show the isotherm models for lead and zinc ions adsorption onto Fe_3O_4/o-MWCNTs surface. The calculated parameters from the Langmuir and Freundlich models are presented in Table 4. Table 4 illustrates that lead and zinc ions adsorption were better fitted for the Langmuir isotherm model with higher R^2 values than the Freundlich model. The correlation coefficient (R^2) of Langmuir isotherm model for zinc ions was 0.989, which was higher than Freundlich isotherm model ($R^2 = 0.821$). Therefore, Langmuir isotherm model correlated better than Freundlich isotherm, indicating that zinc ions adsorption did not interact with itself and was a monolayer adsorption process. Similar phenomenon can be obtained from lead ions adsorption. The maximum adsorption capacities (q_m) of Fe_3O_4/o-MWCNTs were 67.25 and 3.759 mg/g for lead and zinc ions, respectively. This indicated that this method will be highly efficient and economically viable applied for commercial applications. The R_L (0.633 and 0.713) were between 0 and 1, indicating that lead and zinc ions adsorption on Fe_3O_4/o-MWCNTs surface was favorable [42].

3.5.4. Comparison with other adsorbent

The comparison of our experiment's adsorbent with some other adsorbents for the adsorption of Pb^{2+} and Zn^{2+} is listed in Table 5. The adsorption capacity of Fe_3O_4/o-MWCNTs for Pb^{2+} was 2 and 1.2 times as strong as that of activated carbon and sugarcane bagasse/multi-walled CNT, respectively. Madhava Rao et al. [3] reported adsorption capacity of activated carbon was 25.5 and 24.1 mg/ g for Pb^{2+} and Zn^{2+}, respectively. The maximum lead adsorption capacity of sugarcane bagasse/multi-walled CNT was 56.6 mg/g.

3.6. Lead and zinc ions adsorption mechanisms

Functional groups, such as hydroxy, were produced on the surface of Fe_3O_4/o-MWCNTs and

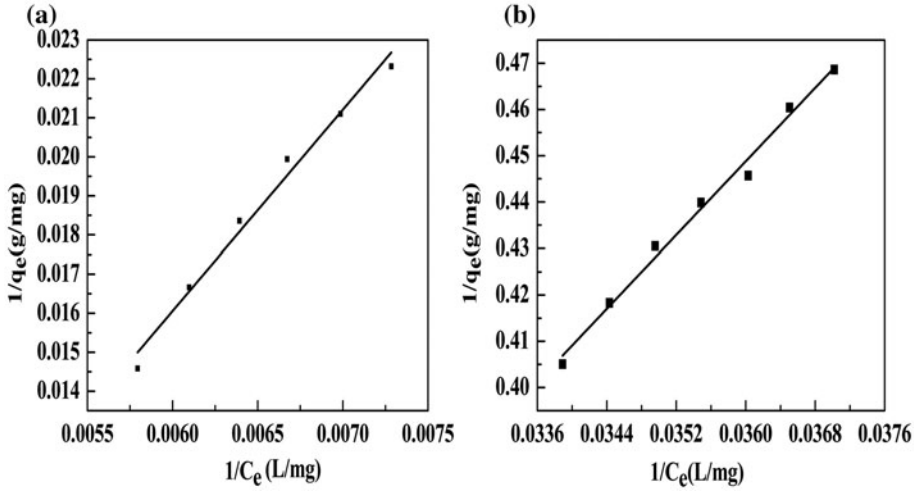

Fig. 11. Langmuir isotherm of lead (a) and zinc (b) adsorption on Fe_3O_4/o-MWCNTs surface.

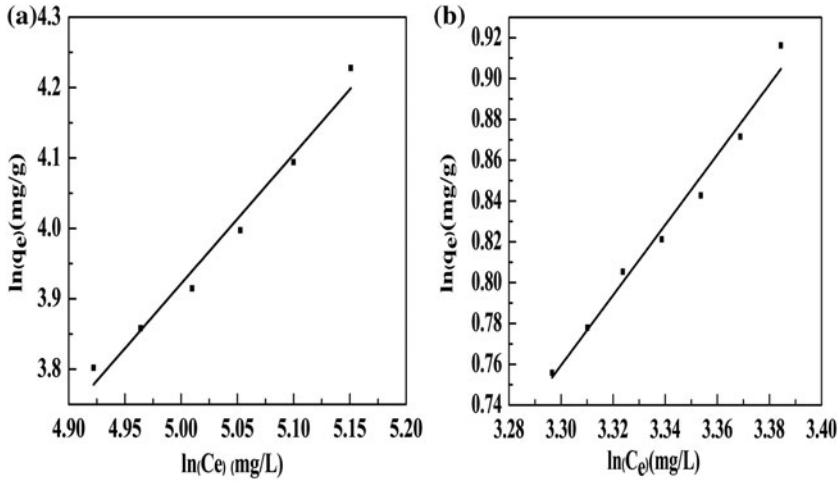

Fig. 12. Freundlich isotherm of lead (a) and zinc (b) adsorption on Fe_3O_4/o-MWCNTs surface.

Table 4
Parameters of Langmuir and Freundlich isotherm models

	Langmuir				Freundlich		
	q_m (mg/g)	b (L/mg)	R_L	R^2	K_f [(mg)$^{1-1/n}$(L)$^{1/n}$/g]	n	R^2
Pb^{2+}	67.25	0.0029	0.633	0.983	0.005	0.544	0.974
Zn^{2+}	3.759	0.013	0.713	0.989	0.014	0.58	0.821

Table 5
Comparison of the published methods for Zn^{2+}, Pb^{2+} determination with different adsorbents

	Adsorbents	q_m (mg/g)	Refs.
Zn^{2+}, Pb^{2+}	Activated carbon	25.5 (Pb^{2+}), 24.1 (Zn^{2+})	[3]
Pb^{2+}	Sugarcane bagasse/multi-walled carbon nanotube	56.6	[35]
Zn^{2+}, Pb^{2+}	Fe_3O_4/o-MWCNTs	67.25 (Pb^{2+}), 3.759 (Zn^{2+})	This experiment

capable of creating a network with water molecules, heavy metal ions by hydrogen bonds, and van der Waals forces. The aggregated pores can be compared to mesopore forms and provided extensive external surface areas. In addition, the adsorption of lead and zinc with oxygenous functional groups can be explained by the ability of functional groups to form complex when in contact with metal ions. The oxygen atoms of these functional groups donated their single pair of electrons to the metal ions, which consequently increased the cation exchange capacity of metal ions. Chemical bonds' interactions between metal ions and acidic functional Fe_3O_4/o-MWCNTs were also responsible for the adsorption [17,43]. Fe_3O_4, which was on the surface of MWCNTs, was not only responsible for separating Fe_3O_4/o-MWCNTs from the aqueous phase, but was also a type of adsorption nanoparticles. It was reported that Fe_3O_4 nanoparticles prepared in the aqueous phase were covered with a number of hydroxy (−OH) groups. Consequently, it was inferred that lead and zinc ions could be immobilized directly on the surface of Fe_3O_4 with −OH groups [44,45].

It was noticeable that adsorption capacity for Pb^{2+} was higher than Zn^{2+}, which may affect surface-binding energy and interactions or the accessibility of centers. The hydrophilic character of functionalized surfaces (strong electronegativity) can increase the affinity with positively charged particles, such as lead and zinc ions. Electronegativity was in the following order: $Pb^{2+} > Zn^{2+}$ (2.33 and 1.65, respectively). This order agreed well with the experimental affinities for

binding and adsorption on Fe_3O_4/o-MWCNTs surface. Because lead ion was predominantly adsorbed (inner-sphere complexation), it can be expected that increasing amount and more strongly bonded lead ions reduced the numbers of adsorption sites for zinc ions adsorption [46]. The lower zinc adsorption capacity might be due to its lower tendency to form hydrolysis products and the fact that zinc ions did not compete effectively for variable charge surfaces.

4. Conclusions

In this study, Fe_3O_4/o-MWCNTs were synthesized and used for simultaneously removing lead and zinc ions from aqueous solutions. TEM provided the evidence that Fe_3O_4 nanoparticles of 10 nm were loaded on the surface of the MWCNTs. The results of XRD, EDS, and XPS further confirmed that the nanoparticles were Fe_3O_4. FTIR spectra showed that evaporating acid purification method produced oxygenic groups on the surface of MWCNTs. The saturation magnetization of Fe_3O_4/o-MWCNTs was 50.10 emu/g. It indicated that Fe_3O_4/o-MWCNTs had strong magnetism and can fast separate from aqueous solutions. The kinetics data were well fitted with the pseudo-second-order kinetics model, suggesting that the rate-limiting step was chemical sorption rather than diffusion. The Langmuir isotherm model fitted the experiment data more closely than the Freundlich isotherm model. Therefore, the prepared Fe_3O_4/o-MWCNTs displayed the key advantages of excellent dispersion in aqueous solution, separation convenience, and high adsorption capacity, implying their potential for the effective removal of heavy metals from aqueous solution.

Acknowledgments

The authors are grateful for financial support from the National Natural Science Foundation of China (51304101) and open fund of the Laboratory of Advanced Processing and Recycling of Non-ferrous Metal in the Lanzhou University of Technology.

Nomenclature

- q_t — the quantity of metal ions adsorbed by per unit mass at time t (mg/g)
- C_0 — the initial concentration of metal ion (mg/L)
- C_t — the concentration of the metal ion at time t (mg/L)
- m — the mass of the adsorbent (g)
- V — the volume of the metal ion solution (L)
- k_1 — the pseudo-first-order adsorption rate coefficient (1/min)
- q_e — the values of amount adsorbed per unit mass at equilibrium (mg/g)
- t — time (min)
- k_2 — the pseudo-second-order rate constant (g/mg/ min)
- K_{id} — the intraparticle diffusion rate constant ($mg/g/min^{0.5}$)
- C_i — a constant proportional to the thickness of the boundary layer (mg/g)
- F — the ratio of adsorption capacity at any time and equilibrium (dimensionless)
- K_{fd} — the film diffusion rate coefficient (1/min)
- q_m — the maximum adsorption capacity (mg/g)
- b — energy of adsorption (L/mg)
- R_L — equilibrium parameter (dimensionless)
- K_f — Freundlich constants related to the adsorption capacity [$(mg)^{1-1/n}(L)^{1/n}/g$]
- n — Freundlich constants related to adsorption intensity (dimensionless)

References

[1] A. Stafiej, K. Pyrzynska, Adsorption of heavy metal ions with carbon nanotubes, Sep. Purif. Technol. 58 (2007) 49–52.
[2] M.A. Salam, Coating carbon nanotubes with crystalline manganese dioxide nanoparticles and their application for lead ions removal from model and real water, Colloids Surf., A: Physicochem. Eng. Aspects 419 (2013) 69–79.
[3] M. Madhava Rao, G.P. Chandra Rao, K. Seshaiah, N.V. Choudary, M.C. Wang, Activated carbon from *Ceiba pentandra* hulls, an agricultural waste, as an adsorbent in the removal of lead and zinc from aqueous soluions, Waste Manage. 28 (2008) 849–858.
[4] S. Iijima, Helical microtubules of graphitic carbon, Nature 354 (1991) 56–58.
[5] C.L. Chen, X.K. Wang, Adsorption of Ni(II) from aqueous solution using oxidized multiwall carbon nanotubes, Ind. Eng. Chem. Res. 45 (2006) 9144–9149.
[6] S.Q. Song, R.C. Rao, H.X. Yang, H.D. Liu, A.M. Zhang, Facile synthesis of Fe_3O_4/MWCNTs by spontaneous redox and their catalytic performance, Nanotechnology 21 (2010) 1–6.
[7] S.X. Xu, L. Tang, C. Bi, X.X. Wang, Y. Lv, A cataluminescence gas sensor for ammonium sulfide based on Fe_3O_4-carbon nanotubes composite, Luminescence 25 (2010) 294–299.
[8] L.Q. Jiang, L. Gao, Carbon nanotubes-magnetite nanocomposites from solvothermal processes: Formation, characterization, and enhanced electrical properties, Chem. Mater. 15 (2003) 2848–2853.
[9] Y.T. Shih, K.Y. Lee, Y.S. Huang, Characterization of iridium dioxide-carbon nanotube nanocomposites grown onto graphene for supercapacitor, J. Alloys Compd. 619 (2015) 131–137.
[10] H.X. Wu, G. Liu, Y.M. Zhuang, D.M. Wu, H.Q. Zhang, H. Yang, H. Hu, S.P. Yang, The behavior after intravenous injection in mice of multiwalled carbon nanotube/Fe_3O_4 hybrid MRI contrast agents, Biomaterials 32 (2011) 4867–4876.

[11] G.D. Tarigh, F. Shemirani, Magnetic multi-wall carbon nanotube nanocomposite as an adsorbent for preconcentration and determination of lead(II) and manganese(II) in various matrices, Talanta 115 (2013) 744–750.
[12] G.D. Vuković, A.D. Marinković, M. Čolić, M.Đ. Ristić, R. Aleksić, A.A. Perić-Grujić, P.S. Uskoković, Removal of cadmium from aqueous solutions by oxidized and ethylenediamine-functionalized multi-walled carbon nanotubes, Chem. Eng. J. 157 (2010) 238–248.
[13] G.D. Vuković, A.D. Marinković, S.D. Škapin, M.Đ. Ristić, R. Aleksić, A.A. Perić-Grujić, P.S. Uskoković, Removal of lead from water by amino modified multi-walled carbon nanotubes, Chem. Eng. J. 173 (2011) 855–865.
[14] C. Li, X. Xu, C.L. Bao, H.F. Wang, L. Liu, X.T. Liu, Adsorption of Au(III) and Pd(II) in solution of 2,2′-diaminodiethylamine modified multi-walled carbon nanotubes, Chem. J. Chin. U. 33 (2012) 586–590.
[15] M.A. Atieh, Removal of chromium(VI) from polluted water using carbon nanotubes supported with activated carbon, Energy Policy 4 (2011) 281–293.
[16] M.A. Salam, R.M. Mohamed, Removal of antimony (III) by multi-walled carbon nanotubes from model solution and environmental samples, Chem. Eng. Res. Des. 91 (2013) 1352–1360.
[17] S. Rosenzweig, G.A. Sorial, E. Sahle-Demessie, J. Mack, Effect of acid and alcohol network forces within functionalized multiwall carbon nanotubes bundles on adsorption of copper(II) species, Chemosphere 90 (2013) 395–402.
[18] S.T. Yang, Z.Q. Guo, G.D. Sheng, X.K. Wang, Application of a novel plasma-induced CD/MWCNT/iron oxide composite in zinc decontamination, Carbohydr. Polym. 90 (2012) 1100–1105.
[19] M.A. Salam, G. Al-Zhrani, S.A. Kosa, Simultaneous removal of copper(II), lead(II), zinc(II) and cadmium (II) from aqueous solutions by multi-walled carbon nanotubes, C.R. Chim 15 (2012) 398–408.
[20] X.J. Peng, Z.K. Luan, Z.C. Di, Z.G. Zhang, C.L. Zhu, Carbon nanotubes-iron oxides magnetic composites as adsorbent for removal Pb(II) and Cu(II) from water, Carbon 43 (2005) 880–883.
[21] W. Zhao, L.J. Zhu, Y.L. Lu, L.Q. Zhang, R.H. Schuster, W.C. Wang, Magnetic nanoparticles decorated multi-walled carbon nanotubes by bio-inspired poly (dopamine) surface functionalization, Synth. Met. 169 (2013) 59–63.
[22] C. Zhang, J.H. Sui, J. Li, Y.L. Tang, W. Cai, Efficient removal of heavy metal ions by thiol-functionalized superparamagnetic carbon nanotubes, Chem. Eng. J. 210 (2012) 45–52.
[23] Y.X. Cheng, Y.J. Liu, J.J. Huang, K. Li, Y.Z. Xian, W. Zhang, L.T. Jin, Amperometric tyrosinase biosensor based on Fe_3O_4 nanoparticles-coated carbon nanotubes nanocomposite for rapid detection of coliforms, Electrochim. Acta 54 (2009) 2588–2594.
[24] B.P. Jia, L. Gao, J. Sun, Self-assembly of magnetite beads along multiwalled carbon nanotubes via a simple hydrothermal process, Carbon 45 (2007) 1476–1481.
[25] Z. Liu, J. Wang, D.H. Xie, G. Chen, Polyaniline-coated Fe_3O_4 nanoparticle-carbon-nanotube composite and its application in electrochemical biosensing, Small 4 (2008) 462–466.
[26] V.K. Gupta, S. Agarwal, T.A. Saleh, Synthesis and characterization of alumina-coated carbon nanotubes and their application for lead removal, J. Hazard. Mater. 185 (2011) 17–23.
[27] G.D. Sheng, J.X. Li, D.D. Shao, J. Hu, C.L. Chen, Y.X. Chen, X.K. Wang, Adsorption of copper(II) on multi-walled carbon nanotubes in the absence and presence of humic or fulvic acids, J. Hazard. Mater. 178 (2010) 333–340.
[28] H.Y. Zhu, Y.Q. Fu, R. Jiang, J. Yao, L. Liu, Y.W. Chen, L. Xiao, G.M. Zeng, Preparation, characterization and adsorption properties of chitosan modified magnetic graphitized multi-walled carbon nanotubes for highly effective removal of a carcinogenic dye from aqueous solution, Appl. Surf. Sci. 285 (2013) 865–873.
[29] H.F. Zhou, C. Zhang, H.Q. Li, Z.J. Du, Decoration of Fe_3O_4 nanoparticles on the surface of poly(acrylic acid) functionalized multi-walled carbon nanotubes by covalent bonding, J. Polym. Sci. Part A: Polym. Chem. 48 (2010) 4697–4703.
[30] J.H. Deng, X.H. Wen, Q.N. Wang, Solvothermal *in situ* synthesis of Fe_3O_4-multi-walled carbon nanotubes with enhanced heterogeneous Fenton-like activity, Mater. Res. Bull. 47 (2012) 3369–3376.
[31] C. Cunha, S. Panseri, D. Iannazzo, A. Piperno, A. Pistone, M. Fazio, A. Russo, M. Marcacci, S. Galvagno, Hybrid composites made of multiwalled carbon nanotubes functionalized with Fe_3O_4 nanoparticles for tissue engineering applications, Nanotechnology 23 (2012) 1–10.
[32] M. Bystrzejewski, K. Pyrzyńska, A. Huczko, H. Lange, Carbon-encapsulated magnetic nanoparticles as separable and mobile sorbents of heavy metal ions from aqueous solutions, Carbon 47 (2009) 1201–1204.
[33] J.N. Gao, X.Z. Ran, C.M. Shi, H.M. Cheng, T.M. Cheng, Y.P. Su, One-step solvothermal synthesis of highly water-soluble, negatively charged superparamagnetic Fe_3O_4 colloidal nanocrystal clusters, Nanoscale 5 (2013) 7026–7033.
[34] S.Y. Mak, D.H. Chen, Binding and sulfonation of poly (acrylic acid) on iron oxide nanoparticles: A novel, magnetic, strong acid cation nano-adsorbent, Macromol. Rapid Commun. 26 (2005) 1567–1571.
[35] I.A.A. Hamza, B.S. Martincigh, J.C. Ngila, V.O. Nyamori, Adsorption studies of aqueous Pb(II) onto a sugarcane bagasse/multi-walled carbon nanotube composite, Phys. Chem. Earth Parts A/B/C 66 (2013) 157–166.
[36] C.Y. Lu, H.S. Chiu, Adsorption of zinc(II) from water with purified carbon nanotubes, Chem. Eng. Sci. 61 (2006) 1138–1145.
[37] I. Persson, Hydrated metal ions in aqueous solution: How regular are their structures? Pure Appl. Chem. 82 (2010) 1901–1917.
[38] E. Salehi, S.S. Madaeni, L. Rajabi, A.A. Derakhshan, S. Daraei, V. Vatanpour, Static and dynamic adsorption of copper ions on chitosan/polyvinyl alcohol thin adsorptive membranes: Combined effect of polyethylene glycol and aminated multi-walled carbon nanotubes, Chem. Eng. J. 215–216 (2013) 791–801.
[39] H. Al-Johani, M.A. Salam, Kinetics and thermodynamic study of aniline adsorption by multi-walled carbon nanotubes from aqueous solution, J. Colloid Interface Sci. 360 (2011) 760–767.

[40] W. Plazinski, Applicability of the film-diffusion model for description of the adsorption kinetics at the solid/solution interfaces, Appl. Surf. Sci. 256 (2010) 5157–5163.
[41] I. Langmuir, The adsorption of gases on plane surfaces of glass, mica and platinum, J. Am. Chem. Soc. 40 (1918) 1361–1403.
[42] F. Yu, Y.Q. Wu, J. Ma, C. Zhang, Adsorption of lead on multi-walled carbon nanotubes with different outer diameters and oxygen contents: Kinetics, isotherms and thermodynamics, J. Environ. Sci. 25 (2013) 195–203.
[43] G.X. Zhao, X.M. Ren, X. Gao, X.L. Tan, J.X. Li, C.L. Chen, Y.Y. Huang, X.K. Wang, Removal of Pb(II) ions from aqueous solutions on few-layered graphene oxide nanosheets, Dalton Trans. 40 (2011) 10945–10952.
[44] S.B. Yang, C.L. Chen, Y. Chen, J.X. Li, D.Q. Wang, X.K. Wang, W.P. Hu, Competitive adsorption of Pb^{II}, Ni^{II}, and Sr^{II} Ions on graphene oxides: A combined experimental and theoretical study, ChemPlusChem 80 (2015) 480–484.
[45] X.C. Shen, X.Z. Fang, Y.H. Zhou, H. Liang, Synthesis and characterization of 3-aminopropyltriethoxysilane-modified superparamagnetic magnetite nanoparticles, Chem. Lett. 33 (2004) 1468–1469.
[46] S.B. Yang, J. Hu, C.L. Chen, D.D. Shao, X.K. Wang, Mutual effects of Pb(II) and humic acid adsorption on multiwalled carbon nanotubes/polyacrylamide composites from aqueous solutions, Environ. Sci. Technol. 45 (2011) 3621–3627.